Characterization of Soybean Protein Adhesives Modified by Xanthan Gum

Chen Feng [1],[†], Fang Wang [1],[†], Zheng Xu [2], Huilin Sui [1], Yong Fang [1], Xiaozhi Tang [1] and Xinchun Shen [1],*

[1] Key Laboratory of Grains and Oils Quality Control and Processing, Collaborative Innovation Center for Modern Grain Circulation and Safety, College of Food Science and Engineering, Nanjing University of Finance and Economics, Nanjing 210023, China; 1120160621@stu.nufe.edu.cn (C.F.); wangfang@nufe.edu.cn (F.W.); 1120170689@stu.nufe.edu.cn (H.S.); fangyong10@njue.edu.cn (Y.F.); warmtxz@126.com (X.T.)

[2] Department of Statistics, Quantitative Life Sciences Initiative, University of Nebraska-Lincoln, Lincoln, NE 68583, USA; zheng.xu@unl.edu

* Correspondence: shenxinchun@nufe.edu.cn; Tel.: +86-25-8587-0260

† These authors contributed equally to this work.

check for updates

Abstract: The aim of this study was to provide a basis for the preparation of medical adhesives from soybean protein sources. Soybean protein (SP) adhesives mixed with different concentrations of xanthan gum (XG) were prepared. Their adhesive features were evaluated by physicochemical parameters and an in vitro bone adhesion assay. The results showed that the maximal adhesion strength was achieved in 5% SP adhesive with 0.5% XG addition, which was 2.6-fold higher than the SP alone. The addition of XG significantly increased the hydrogen bond and viscosity, as well as increased the β-sheet content but decreased the α-helix content in the second structure of protein. X-ray diffraction data showed significant interactions between SP molecules and XG. Scanning electron microscopy observations showed that the surface of SP adhesive modified by XG was more viscous and compact, which were favorable for the adhesion between the adhesive and bone. In summary, XG modification caused an increase in the hydrogen bonding and zero-shear viscosity of SP adhesives, leading to a significant increase in the bond strength of SP adhesives onto porcine bones.

Keywords: soybean protein (SP); xanthan gum (XG); adhesion properties; adhesives

1. Introduction

Soybean is widely planted and is an important legume as a predominant plant source for both animal feed protein and cooking oil. Soybean protein (SP) is a major source of vegetable proteins. This protein has been widely applied in many areas, such as effectively improving nutritional values and properties (including changing the gel, emulsification, and rheology) in food manufacturing and processing [1,2]. The application of SP to adhesive materials enhances the values of agricultural products and alleviates environmental problems [3–5]. Recently, the advancement of protein technologies allowed further development of SP functions. SP has been widely studied as raw materials for biomaterials, such as wound dressing films, hydrogels, scaffolds, and bone fillers [6–9]. Previous studies have found that SP-based biomaterials promoted cell adhesion and proliferation and induced osteoblast differentiation [10,11].

Medical adhesives are widely used in clinical medicine, including healing of the fracture, dental restoration, and surgical sutures. The most common medical adhesives are chemical adhesives, such as α-cyanoacrylate. However, the poor biocompatibility, tissue healing impediments,

low biodegradability, and dose dependent tissue necrosis limited their application [12,13]. In addition, environmental unfriendly features were another big concern for chemical adhesives [14]. Recently, bio-adhesive products emerged on the market. For example, fibrin adhesives were applied in the clinic for fracture healing. Fibrin adhesives were extracted from animal or human blood [15]. Therefore, cross viral infection was a major concern [16,17]. Another bio-adhesive was prepared from marine mussels, which was first extracted and identified to have adhesive capacity by Waite et al. [18]. Mussel adhesive has the advantage of low immunogenic qualities, high strength, and durability [19]. However, the low volume of production and high price limited their applications [20,21]. In contrast, adhesives prepared from SP are safer, biodegradable, lower immunogenicity and offer better biocompatibility compared to adhesives prepared from animal proteins. In addition, SP is widely available, renewable, and economic. Thus, SP based adhesives are promising for medical application. However, current adhesives derived from pure SP had poor adhesive performance, which restricted their medical application.

In the past several years, protein modification technologies have been developed that allow the generation of different SP-based adhesives. Previous studies showed that alkali-denatured SP [22] or dopamine grafted SP [23] had superior adhesive properties and water resistance. SP modified with diacetyl tartaric acid increased the bonding strength [24]. In addition, the combination of SP with polysaccharides, such as carrageenan, has been shown to improve the gelling property of SP [25]. Our previous studies found that the modification of SP with polysaccharides (such as guar gum) improved the bond strength of SP [26]. Protein-polysaccharide interactions may be a simple and safe modification for enhanced functional properties of SP. Xanthan gum (XG) is a heteropolysaccharide that consists of D-glucose, D-mannose, and D-glucuronic acid units. It is a pentasaccharide derived from bacteria and fungi [27]. XG has a structure of trisaccharide side chains aligned with the main chain. This structure makes the XG more resilient to heat in acidic and alkaline environments [28]. XG is biodegradable and nontoxic. Moreover, XG has good biocompatibility and is widely available in nature. The addition of XG has been shown to increase the bulk viscosity of SP and affect its surface rheology [29]. In addition, XG also improved the emulsion stability and changed the microstructure of SP [30]. Furthermore, XG increased a liquid's viscosity when added in a small amount at low shear rates [31,32]. However, whether incorporation of XG in SP adhesives improves their adhesion properties is unclear. In the present study, using an in vitro bone adhesion model, the adhesion properties and performance of SP adhesive after adding XG were investigated.

2. Materials and Methods

2.1. Materials

Soybeans and porcine bones were obtained from a local supermarket. XG was purchased from Shanghai Jingchun Biochemical Technology Company (Shanghai, China). Calcium chloride was purchased from Sinopharm Chemical Reagent Co., Ltd. (Shanghai, China). Phosphate-buffered saline (PBS) and Ethyl ether were purchased from Shanghai Bio-engineering Company (Shanghai, China). All reagents were of analytical grade (AR).

2.2. Preparation of Soybean Proteins

The preparation of SP was based on a procedure described previously with minor modifications [33,34]. Briefly, the soy powder was mixed with ethyl ether at a ratio of 1:8 (w/v, g/L). The mixture was then shaken in a thermostatic oscillator (25 °C, 100 r/min) for 9 h for degreasing. The degreased soy powder was dissolved in distilled water (1:10) at pH 8.0, and mixed for 35 min at 45 °C The suspension was centrifuged at 3500× g for 30 min. The pH of supernatant was adjusted 4.6 and centrifuged for 10 min at 3500× g. The precipitate was suspended with water and the pH was adjusted to 7.0. The protein solution was dialyzed against deionized water, freeze-dried, and stored at

−20 °C. The protein content of the SP was measured using the Kjeldahl method following the national standard GB 5009.5-2010 (China) [25].

2.3. Preparation of XG-Modified SP (SP-XG) Adhesives

Different amounts of SP were completely dissolved and constantly stirred in 0.1 mol/L PBS solution (pH 7.6) to obtain 2%, 5% or 8% (*w*/*v*, g/mL) pure SP adhesives. Different amounts of XG were then evenly dispersed into each of the three pure SP adhesives to get 0%, 0.25%, 0.5% or 1% (*w*/*v*, g/mL), respectively. The SP-XG adhesives were incubated in a thermostatic oscillator at 60 °C for 30 min before being quickly cooled to room temperature (25 °C) to obtain the SP-XG adhesives.

2.4. Characterizations of SP-XG Adhesives

2.4.1. Raman Spectroscopic Measurement

Raman spectra of the samples were measured using a laser confocal Raman microscope (Renishaw Company, York, UK) following a procedure described previously [26]. The spectral data were baseline-corrected and normalized to define the intensity of the phenylalanine band at 1003 cm^{-1} as 1. The relative Raman spectral peak strengths of the different samples were analyzed using the Peakfit 4.0 software package (Jandel Scientific).

2.4.2. Fourier Transform Infrared (FTIR) Spectroscopy

FTIR spectra were obtained with a Bruker Tensor-27 FTIR Spectrometer (Bruker Company, Karlsruhe, Germany). Briefly, an SP-XG adhesive sample was ground with potassium bromide (KBr) (1:10) for FTIR analysis. Each sample was scanned 16 times at a resolution of 2 cm^{-1}, and transmission spectra were recorded from 4000 to 600 cm^{-1}. The second derivative and fitted curve were analyzed with the Peakfit 4.0 software package (Jandel Scientific).

2.4.3. X-ray Diffraction (XRD) Analysis

XRD measurements of the lyophilized samples were performed using a D8 Advance X-ray diffractometer (Bruker Company, Karlsruhe, Germany) with a scanning range of 10° to 80° in 2θ according to Chen et al. [26].

2.5. Adhesion Properties of SP-XG Adhesives

2.5.1. Rheological Properties

Zero-shear viscosity measurements of the samples were performed using an Anton Paar MCR302 rheometer (Anton Paar, Graz, Austria) with a parallel plate (PP50, 60 mm plate diameter and 0.5 mm gap) according to Rudolph et al. [35].

2.5.2. Measurement of Tensile Shear Strength Using an In Vitro Adhesives Bonding Model

An in vitro adhesive bonding test using porcine bones was set up as described previously [26]. The tensile shear strength of SP-XG was measured using an Instron testing machine (Model HY-0580, Shanghai Hengyi Precision Instrument Company, Shanghai, China) according to the ASTM D1002 [36] method. The tensile adhesion strength in pascals (kPa = N/m^2) was calculated by dividing the observed maximum loading (N) by the adhesive area (m^2). The mean values of the results from twelve samples were used in our analysis.

2.6. Scanning Electron Microscopy (SEM)

SEM images (TM3000, Hitachi, Tokyo, Japan) were obtained to study the surface morphology of the samples. The freeze-dried samples were coated with a thin layer of gold using an ion sputter coater before being examined and photographed.

2.7. Statistical Analysis

The data were represented as mean ± standard deviation (SD). All data were obtained at least three times. Analysis of variance (ANOVA) and *t*-tests were conducted, and *p*-value < 0.05 was set as statistically significant.

3. Results

3.1. Adhesion Properties of SP-XG Adhesives

3.1.1. Effect of XG on Tensile Shear Strength of SP Adhesives

The addition of 0.25% and 0.5% XG significantly enhanced the adhesion strength of different concentrations of SP adhesives (*p* < 0.05) except 8% SP. However, this enhancement disappeared when 1% XG was added. (Figure 1a). Specifically, after 0.5% XG addition, the adhesion strength of 2% or 5% SP adhesives increased from 33 kPa or 140 kPa to 123 kPa and 361 kPa, respectively. The adhesion strength of 5% SP adhesive with 0.5% XG was the best, which was increased 2.6-fold compared to the raw SP adhesive (*p* < 0.01). Thus, a 5% SP concentration was chosen to perform the subsequent experiments. Importantly, the adhesion strength of 5% SP adhesive with 0.5% XG was significantly greater than the sum of the strengths of 5% SP adhesive alone and 0.5% XG only, indicating a synergistic effect [37]. Interestingly, a special situation was observed that the adhesion strength of 8% SP adhesive decreased slightly after the addition of XG (Figure 1a), which is possibly due to the gelatinization and phase separation that occurred in a high concentration of soy protein with polysaccharide [38]. Zhang et al. found similar results that the addition of sodium carboxymethyl cellulose significantly improved the adhesion strength of low-concentration SP adhesive (2%), but reduced the adhesion strength of high-concentration SP adhesive (10%) [39]. Currently, mussel adhesives and SP adhesives are significant potential candidates for the next generation of medical adhesives. The mussel adhesives extracted from Perna viridis foot had a strength of 135 kPa on ruptured porcine femur, which was greater than the commonly used biomedical fibrin adhesive [40]. A previous study showed that the bond strength of a synthetic co-polypeptide composed of 3,4-dihydroxyphenylalanine on porcine bone was 295 kPa [41]. Therefore, a bone bio-adhesive of SP-XG was higher than the natural P. californica adhesive [42]. Although the SP-XG adhesion strength was still lower than cyanoacrylate adhesive to bone (1.95–8.00 MPa) as shown in a previously published study [43], the adhesive strength of 200 kPa was considered as a practical threadshield for maintaining the bone bond [44]. Therefore, the bone adhesive made by adding 0.5% XG to 5% SP adhesive had great adhesive performance and was one of the best potential candidates for biomedical applications.

3.1.2. Effect of XG on Zero-Shear Viscosity of SP Adhesives

Previous studies have shown that SP and XG were typical shear thinning fluids that showed non-Newtonian behaviors. SP has pseudoplasticity and high viscosity near zero-shear force. As the shear force increases, the solution becomes thinner and the viscosity decreases [45]. In addition, viscosity is an important property that regulates the adhesion behavior and performance. Our previous results indicated that there was a significant positive correlation between the adhesion strength and zero-shear viscosity in SP adhesives when sodium carboxymethyl cellulose was used as a modifying reagent [39]. Our current study showed that the addition of 0.5% XG significantly improved the zero-shear viscosity of the SP adhesive (*p* < 0.05), which led to an increase in the bond strength between the SP adhesive and bones (Figure 1b). However, there was a gelatinization phenomenon in the SP adhesive when 1% XG was added. Although the zero-shear viscosity of the SP adhesive increased sharply, the adhesion between the SP and bones was still decreased.
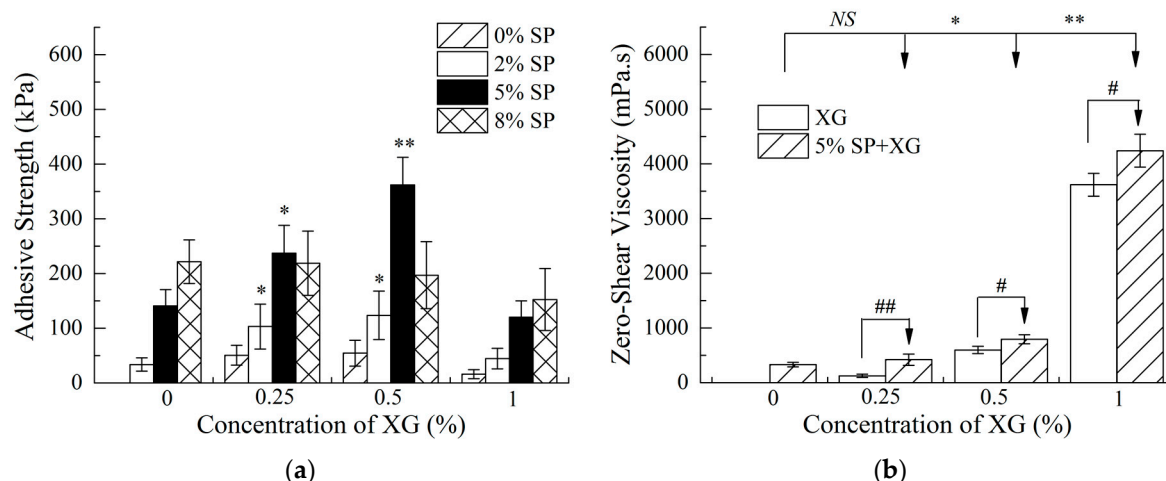
Figure 1. Tensile shear strength (**a**) and zero-shear viscosity (**b**) of soybean protein (SP) adhesives in the presence of xanthan gum (XG). Compared with the control of SP without XG addition, NS indicates no significant difference ($p > 0.05$), * indicates significant difference ($p < 0.05$), and ** indicates extremely significant difference ($p < 0.01$); compared with pure XG, [#] indicates significant difference ($p < 0.05$), and [##] indicates extremely significant difference ($p < 0.01$).

3.2. Characterizations of SP-XG Adhesives

3.2.1. Raman Spectroscopic Analysis

The Raman spectra of 5% SP with varying concentrations of XG were illustrated in Figure 2a. Several major bands in the Raman spectra were identified, which centered at 760 cm^{-1} (tryptophan band), 830 cm^{-1} (tyrosine doublet), 850 cm^{-1} (tyrosine doublet), 1003 cm^{-1} (phenylalanine), 1240 cm^{-1} (amide III), 1450 cm^{-1} (C–H bending), and 1669 cm^{-1} (amide I). A prior study showed that the phenylalanine band at 1003 cm^{-1} was insensitive to conformation or the microenvironment [46]. Therefore, the spectral data were baseline-corrected and normalized using the intensity of the phenylalanine band at 1003 cm^{-1} [47]. The amide I Raman band was used to determine the secondary structural information of the proteins. A quantitative analysis of the secondary structure compositions in the SP-XG adhesives was performed using the Peakfit 4.0 software package. As shown in Table 1, with the increase addition of XG from 0% to 0.5%, the α-helix content decreased significantly ($p < 0.05$) whereas the β-sheet content increased significantly ($p < 0.05$). The contents of the β-turn and random coil were not significantly affected by XG. The protein structural changes in the presence of XG may be related to the increased interaction between XG and SP. Dickinson et al. found that anionic polysaccharides and proteins interacted at pH > pI, resulting in the unfolding of the protein [48]. The α-helix was stabilized mainly by the intramolecular hydrogen bonds between the carbonyl oxygen (–CO) and amino hydrogen (NH–). The adhesives were consisted of flexible and interlaced polymer chains usually showed good adhesion properties, consequently the globular structure had to be destroyed [49]. The reduction in α-helix contributed to the unfolding of the protein molecular structures and enhanced the adhesion strength. The β-sheet is composed of polypeptide chains extending in the protein and formed by intermolecular hydrogen bonding. Compared to the α-helix structure, β-sheet has poor conformational stability [50]. Zhang et al. found that the increase in β-sheet content enhanced the adhesive strength of SP on walnut and cherry [51]. With the decrease in α-helix and the increase in β-sheet in SP-XG, the flexibility of the protein was significantly improved, which was conducive to the interaction and bonding strength between SP and bones. Therefore, the addition of 0.5% XG loosened the molecular structure of the protein. The intramolecular hydrogen bond was converted into an intermolecular hydrogen bond and the active group was partially exposed, thereby enhancing the interaction between the SP adhesives and bones. However, when the XG

concentration was increased from 0.5% to 1%, the α-helix content showed a trend of decrease ($p > 0.05$) and the β-turn content showed a trend of increase ($p > 0.05$).
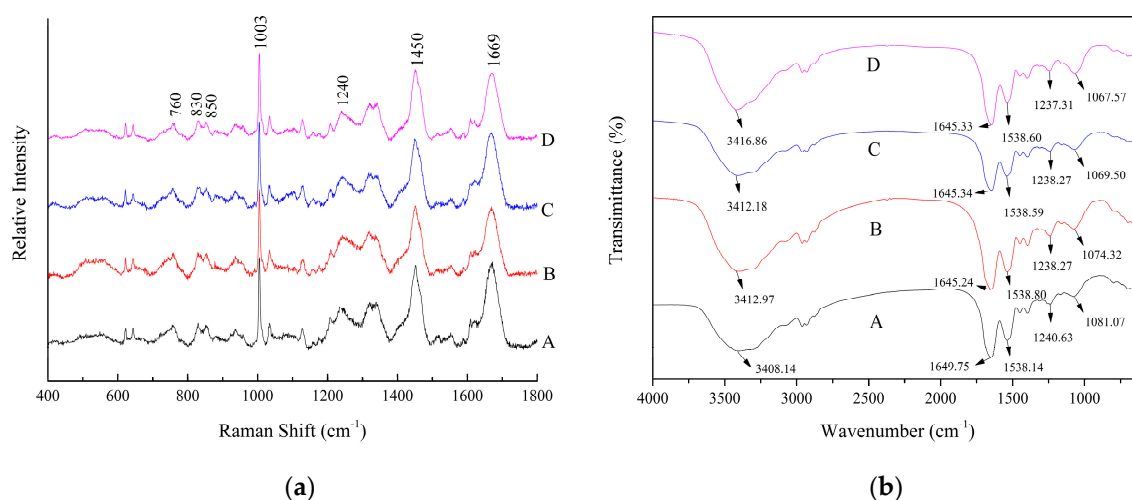

Figure 2. Raman (**a**) and Fourier transform infrared (FTIR) (**b**) spectra of SP adhesives with different concentrations of XG. (A) 5% SP only; (B) 5% SP + 0.25% XG; (C) 5% SP + 0.5% XG; (D) 5% SP + 1% XG.

Table 1. Quantitative analysis of the relative amounts of secondary structure.

XG Concentration (%)	α-Helix	β-Sheet	β-Turn	Random Coil	I_{760}/I_{1003}	I_{850}/I_{830}	N_{buried}	$N_{exposed}$
0	24.17 ± 0.62 [a]	27.68 ± 1.07 [a]	16.63 ± 0.93	31.52 ± 1.31	0.37 ± 0.03	1.09 ± 0.02 [a]	0.21 ± 0.02 [a]	0.79 ± 0.02 [a]
0.25	21.21 ± 1.4 [b]	29.47 ± 1.04 [a]	17.26 ± 0.85	32.06 ± 0.95	0.34 ± 0.02	0.96 ± 0.11 [a]	0.39 ± 0.15 [a]	0.61 ± 0.15 [a]
0.5	18.49 ± 2.05 [bc]	32.68 ± 1.18 [b]	18.27 ± 1.01	30.56 ± 2.07	0.36 ± 0.03	0.8 ± 0.06 [b]	0.6 ± 0.07 [b]	0.4 ± 0.07 [b]
1	18.66 ± 0.69 [c]	33.99 ± 0.46 [b]	16.28 ± 1.27	31.06 ± 1.47	0.35 ± 0.02	0.84 ± 0.03 [b]	0.54 ± 0.04 [b]	0.46 ± 0.04 [b]

Notes: Values are given as mean ± standard deviation; Different letters ([a], [b], [c]) in the same column indicate significant differences ($p < 0.05$, $n = 3$).

Normalized intensities of the 760 cm^{-1} (tryptophan) band and tyrosyl doublet at 850/830 cm^{-1} and molar number of "buried" and "exposed" tyrosine residues of SP adhesives based on Raman spectra, as shown in Figure 2a; a–c Different superscript letters in the same column indicate significant differences ($p < 0.05$).

The changes in several Raman bands provided information regarding the hydrophobic interactions and the tertiary structure of proteins, including tryptophan, tyrosyl doublets, and aliphatic hydrophobic residues. Previous studies have shown that the band at 760 cm^{-1} was reported to be the tryptophan vibration [51] and the change in the band intensity of 760 cm^{-1} showed the exposure of hydrophobic residues. However, no significant differences ($p > 0.05$) were observed in the normalized intensity of the Raman band near 760 cm^{-1} between the control (SP only) and the SP-XG adhesives (Table 1). The ratio of tyrosyl double bonds at 850 and 830 cm^{-1} is a good indicator of the hydrogen bonding of phenolic hydroxyl groups, which reflects the status of the exposed and buried tyrosyl residues in the protein. Our current study showed that the ratio of I_{850}/I_{830} was decreased from 1.09 to 0.96 ($p > 0.05$) or 0.8 ($p < 0.05$), respectively, when the concentration of XG was increased from 0% to 0.25% or 0.5% (Table 1). This suggests that the addition of XG decreased the exposure of tyrosine residues in the SP adhesives, consequently increased the formation of buried hydrogen bonds. A prior study demonstrated that, when the value of I_{850}/I_{830} is in the range of 0.5 to 1.25, the number of buried and exposed tyrosine residues were calculated using the following formulae: $0.5N_{buried} + 1.25N_{exposed} = I_{850}/I_{830}$ and $N_{buried} + N_{exposed} = 1$ [52]. Our analysis showed that after incorporation of 0.5% XG, the "exposed" hydrogen bonds associated with tyrosine residues in the SP adhesives were switched to "buried" hydrogen bonds, indicating enhanced SP intramolecular hydrogen bonding. Similar results have been reported by Chen et al. [26].

3.2.2. FTIR Spectroscopy

Typical FTIR spectra of 5% SP adhesives modified with varying concentrations of XG were presented in the Figure 2b. The IR spectral peaks of SP at 1649 cm^{-1}, 1538 cm^{-1}, and 1240 cm^{-1} were assigned to amide I, amide II, and amide III, respectively [53]. The vibration of amide I represents the secondary structure of the protein skeleton and is often used for the quantitative analysis of different secondary structures. Deconvoluted spectra of the amide I band were used for curve fitting, as shown in Figure 3. The band at 1660–1650 cm^{-1} was assigned to α-helix. The bands at 1640–1610 cm^{-1} and 1700–1680 cm^{-1} were assigned to β-sheet [54]. The data were normalized by dividing the corresponding peak intensity by that of, an internal reference, the C–H peak (2930 cm^{-1}). With the addition of XG, the absorption peak at 1651 cm^{-1} was decreased, whereas the peaks at 1621 cm^{-1} and 1635 cm^{-1} were increased, indicating a decrease in α-helix and an increase in β-sheet (Table 2), which were consistent to the results of Raman spectroscopy. With XG addition, the absorption peak at 1666 cm^{-1}, assigned to turn structure, was significantly increased, indicating the increase of turn structure in SP. A similar result was obtained in the Raman analysis, which showed a trend of increase of the β-turn structure in SP with the addition of 0.5% XG. With the amide I and amide III bands were shifted to the lower frequencies, H-bonding was enhanced [55]. Therefore, we concluded that incorporation of XG increased the hydrogen bonding in the secondary structure of SP.
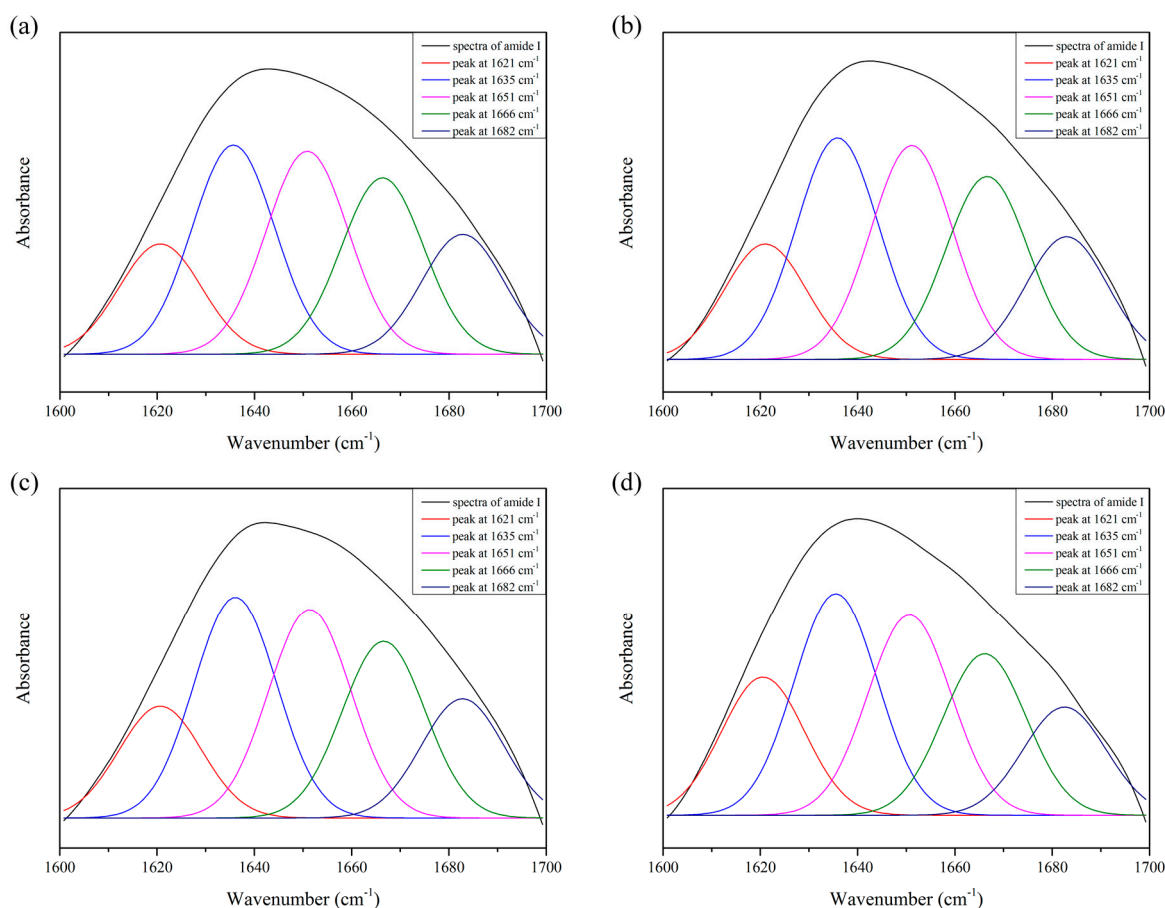

Figure 3. Original spectrum (black) and curve-fitting spectra of amide I for SP adhesives with different concentration of XG. (**a**) 5% SP only; (**b**) 5% SP + 0.25% XG; (**c**) 5% SP + 0.5% XG; (**d**) 5% SP + 1% XG.

Table 2. Normalized intensities of the characteristic absorption peaks for SP adhesives with different concentrations of XG based on FTIR.

XG Concentration (%)	1666/2930 cm^{-1}	1651/2930 cm^{-1}	1635/2930 cm^{-1}	1621/2930 cm^{-1}
0	2.257 ± 0.093 [a]	2.499 ± 0.088 [a]	2.372 ± 0.083 [a]	1.212 ± 0.079 [a]
0.25	2.455 ± 0.081 [b]	2.402 ± 0.072 [a]	2.411 ± 0.118 [a]	1.264 ± 0.072 [a]
0.5	2.497 ± 0.107 [b]	2.303 ± 0.075 [b]	2.572 ± 0.092 [b]	1.381 ± 0.066 [b]
1	2.488 ± 0.096 [b]	2.241 ± 0.121 [b]	2.690 ± 0.132 [b]	1.424 ± 0.097 [b]

Notes: The data were derived from Figures 2b and 3; [a], [b] Different superscript letters in the same column indicate significant differences ($p < 0.05$).

The bands between 3500–3300 cm^{-1} represented the overlapping of the stretching vibration of the OH groups and NH groups. After adding XG, the absorption of O–H stretching vibration was shifted from 3408 cm^{-1} to 3416 cm^{-1}, indicating interactions between the hydroxyl groups of XG and the amino groups of SP [27]. In addition, the down shift of the band from 1081 cm^{-1} to 1067 cm^{-1} confirmed the formation of hydrogen bonding interactions between SP and XG, since hydrogen bonding could lower the frequency of stretching vibrations [56]. However, there was a gelatinization phenomenon in the SP adhesive when 1% XG was added. Therefore, although the hydrogen bonding increased continuously, the adhesion between the SP and bones was decreased.

3.2.3. X-ray Diffraction (XRD) of SP-XG

XRD analysis provides a clue regarding the crystallinity of SP in SP adhesives with XG-blend microspheres to understand the compatibility of blends. Typical XRD spectra of pure XG (a), SP, and SP-XG (b) were showed in the Figure 4. The diffraction peaks of the XG crystal plane were at 2θ, which equaled to 28°, 32°, 46°, 57°, 66°, and 75°, respectively, whereas for SP adhesives in the presence of XG, the diffraction peak at 2θ = 28° was not observed and the intensity of the peak at 2θ = 32° was decreased (Figure 4b insert Curves B and C), indicating good miscibility and interactions between XG and the SP molecules. At a relative high concentration (ex. 0.5%), XG addition interfered with the arrangement of protein molecular chains in the SP adhesive, facilitating the unfolding of polypeptide chains, which led to a structure that was more amorphous and less crystallized. Li et al. found that the addition of Arabic gum could decrease the crystallinity of peanut protein isolate, promote the unfolding of protein structures, and facilitate the protein-polysaccharide interaction by interfering with the protein chain arrangement [57]. Moreover, with the addition of 0.5% XG, the diffraction peaks were shifted to large angles (high theta values) (Figure 4b insert). Based on Bragg's law, with the increase of scattering angle, the interplanar distance was decreased, indicating the changes in the SP structure and the unfolding of SP. These results confirmed the analysis of the Raman and FTIR results discussed above, that is, XG addition changed the protein secondary structure of SP adhesives, and the protein molecular structures tended to be unfolded, which favored the interactions between XG and SP molecules and good miscibility of XG and SP. However, when the concentration of XG was up to 1%, the diffraction peak shifted back to a smaller angle (a low theta value) and the intensity of the crystallization zone at 2θ = 32° increased (Figure 4b insert), suggesting that the presence of XG at high concentrations could cause an increase in the interplanar distance and the crystallinity. A previous study showed that there is a negative correlation between adhesive property and crystallinity [58]. Therefore, the bond strength of SP adhesives first increased with the increase of XG concentration and then decreased after reaching a peak.
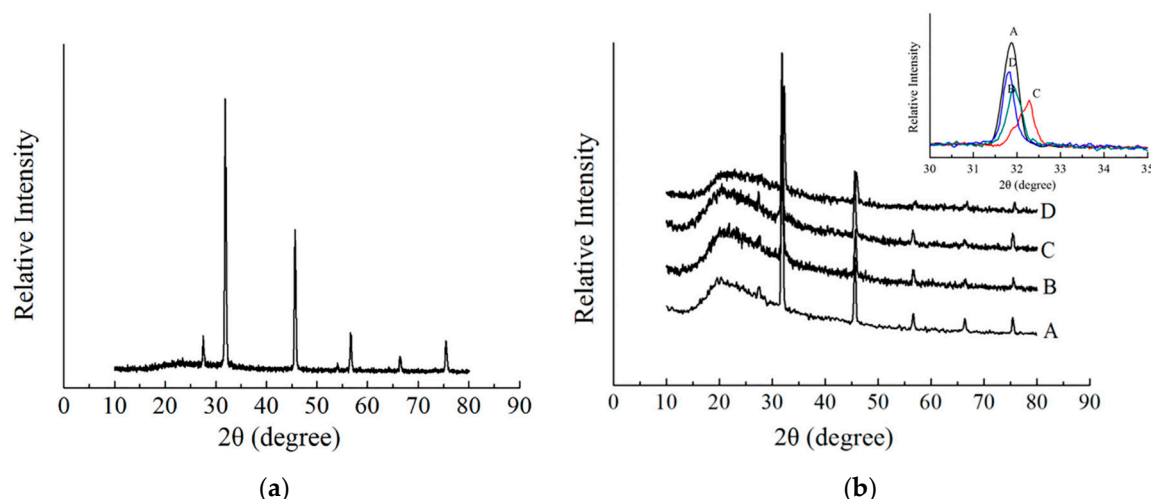
Figure 4. X-ray diffraction spectrum of 0.5% XG (**a**) and X-ray diffraction spectra of SP adhesives with different concentrations of XG (**b**). (A) 5% SP only; (B) 5% SP + 0.25% XG; (C) 5% SP + 0.5% XG; (D) 5% SP + 1% XG.

3.3. Scanning Electron Microscopy (SEM) Analysis of SP-XG Adhesives

The surface morphology of SP-XG adhesives were examined using SEM analysis. The results showed that the surface morphology of these adhesives varied in coarseness with different amount of XG being added (Figure 5). The pure SP adhesive showed a smooth and uniform surface. As the XG concentration increased from 0 to 0.25% or 0.5%, the density of the SP adhesive was enhanced, and a dense and uniform texture appeared on the surface of the SP adhesive, indicating more compact and more amorphous structure [57]. This might facilitate the interaction of SP adhesive with bone. The microstructures of polysaccharide-protein mixed gels were classified into homogeneous and phase-separated [59]. The increase in polysaccharide concentration led to a high degree of phase separation, therefore, high concentrations (1%) of XG split the SP adhesive surfaces and made them became less uniform, indicating the gelatinization and phase separation of the SP adhesives, leading to decreased bonding strength. As shown in Figure 1b, when 1% XG was added, the zero-shear viscosity of the SP adhesive increased sharply, which suggested that there was gelatinization and phase separation in the SP adhesive with the addition of 1% XG. Our XRD analysis indicated that the presence of 1% XG led to an increase in the interplanar distance and the crystallinity in the SP adhesives. The interplanar distance is an important parameter that reflects the intermolecular interactions, and is negatively correlated with the intermolecular interactions [60]. In the protein-polysaccharide mixtures, the intermolecular interaction has been positively correlated with miscibility [61]. Our results demonstrated that the addition of 1% XG led to a decrease of intermolecular interaction and, consequently, a reduction in the miscibility of the SP adhesives. Therefore, these observations were consistent with the results of zero-shear viscosity measurements and confirmed the conclusion from the XRD analysis that the addition of 1% XG led to the formation of new crystals in the SP and decreased the miscibility in the SP adhesives.
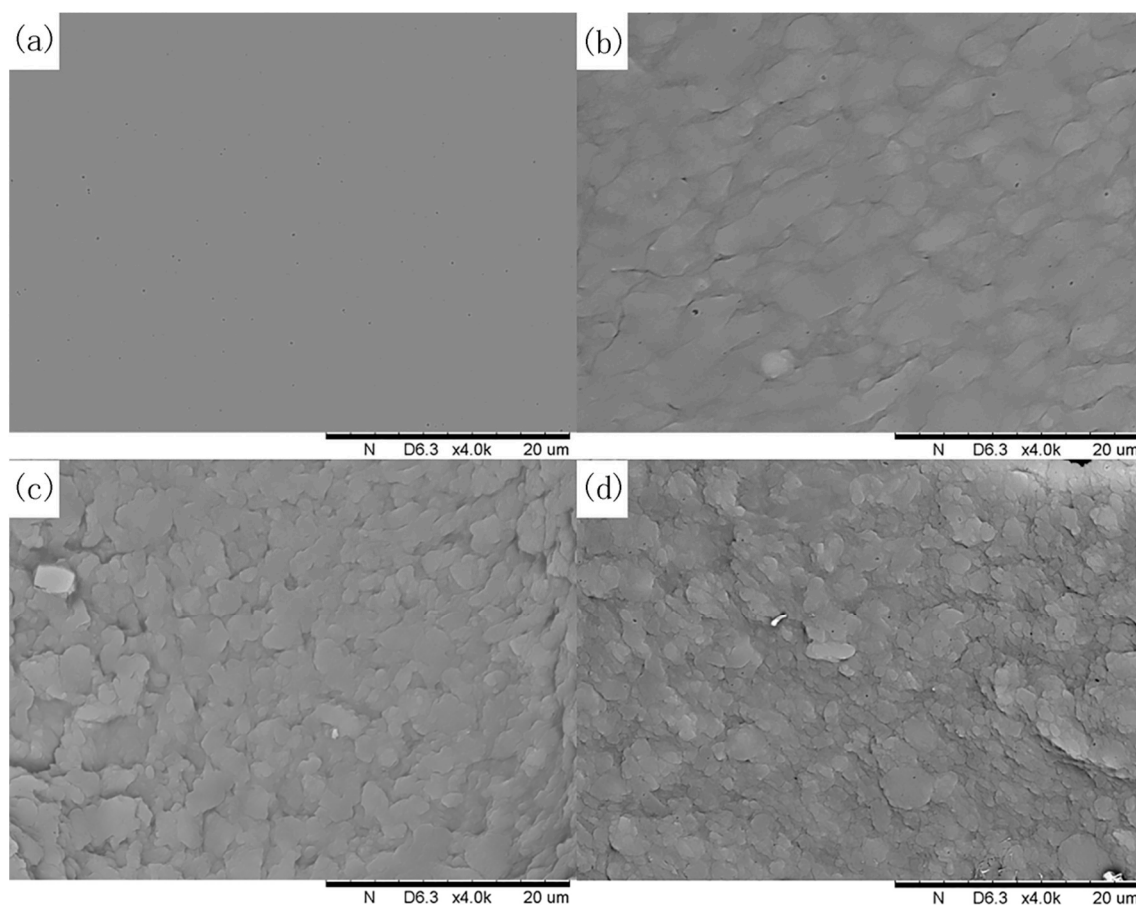
Figure 5. Scanning electron microscope (SEM) images of SP adhesives with the addition of XG at different concentrations: (**a**) 5% SP only; (**b**) 5% SP + 0.25% XG; (**c**) 5% SP + 0.5% XG; (**d**) 5% SP + 1% XG.

4. Conclusions

The addition of 0.5% XG increased the hydrogen bonding of the SP adhesives, which resulted in significant changes in their secondary structure, including a decline in α-helix content and an increase in β-sheet content, both of which indicated unfolding of protein molecules. The structural changes favored a tendency of the protein molecules to be loosened, resulting in the formation of an amorphous structure with a stronger glue network. The increase in the hydrogen bonding and zero-shear viscosity of SP-XG adhesives led to a significant increase in their bond strength with bones. Consequently, SP-XG adhesives have a great potential being applied in medical fields. Future studies will be focused on the effect of SP-XG adhesives on the quality of fracture healing using histological, biomechanical, and micro computed tomography methods in animal studies.

References

1. Machado, V.G.; Hirata, T.A.M.; Menegalli, F.C. Agglomeration of soy protein isolate in a pulsed fluidized bed: Experimental study and process optimization. *Powder Technol.* **2014**, *254*, 248–255. [CrossRef]

2. Han, Y.; Yu, M.; Wang, L. Preparation and characterization of antioxidant soy protein isolate films incorporating licorice residue extract. *Food Hydrocolloids* **2018**, *75*, 187–199. [CrossRef]

3. Lin, Q.; Chen, N.; Bian, L.; Fan, M. Development and mechanism characterization of high performance soy-based bio-adhesives. *Int. J. Adhes. Adhes.* **2012**, *34*, 11–16. [CrossRef]

4. Ayyıldız, S.N.; Ayyıldız, A. Cyanoacrylic tissue glues: Biochemical properties and their usage in urology. *Turk. J. Urol.* **2017**, *43*, 14–24. [CrossRef] [PubMed]

5. Wang, L.; Wu, M.; Liu, H.M. Emulsifying and physicochemical properties of soy hull hemicelluloses-soy protein isolate conjugates. *Carbohydr. Polym.* **2017**, *163*, 181–190. [CrossRef] [PubMed]

6. Peles, Z.; Zilberman, M. Novel soy protein wound dressings with controlled antibiotic release: Mechanical and physical properties. *Acta Biomater.* **2012**, *8*, 209–217. [CrossRef] [PubMed]

7. Chien, K.B.; Chung, E.J.; Shah, R.N. Investigation of soy protein hydrogels for biomedical applications: Materials characterization, drug release, and biocompatibility. *J. Biomater. Appl.* **2014**, *28*, 1085–1096. [CrossRef] [PubMed]

8. Chien, K.B.; Aguado, B.A.; Bryce, P.J.; Shah, R.N. In vivo acute and humoral response to three-dimensional porous soy protein scaffolds. *Acta Biomater.* **2013**, *9*, 8983–8990. [CrossRef] [PubMed]

9. Merolli, A.; Nicolais, L.; Ambrosio, L.; Santin, M. A degradable soybean-based biomaterial used effectively as a bone filler in vivo in a rabbit. *Biomed. Mater.* **2010**, *5*, 015008. [CrossRef] [PubMed]

10. Silva, G.A.; Vaz, C.M.; Coutinho, O.P.; Cunha, A.M.; Reis, R.L. In vitro degradation and cytocompatibility evaluation of novel soy and sodium caseinate-based membrane biomaterials. *J. Mater. Sci. Mater. Med.* **2003**, *14*, 1055–1066. [CrossRef] [PubMed]

11. Santin, M.; Morris, C.; Standen, G.; Nicolais, L.; Ambrosio, L. A new class of bioactive and biodegradable soybean-based bone fillers. *Biomacromolecules* **2007**, *8*, 2706–2711. [CrossRef] [PubMed]

12. Bouten, P.J.; Zonjee, M.; Bender, J.; Yauw, S.T.; van Goor, H.; van Hest, J.C.; Hoogenboom, R. The chemistry of tissue adhesive materials. *Prog. Polym. Sci.* **2014**, *39*, 1375–1405. [CrossRef]

13. Benthien, J.P.; Russlies, M.; Behrens, P. Investigating the effects of bone cement, cyanoacrylate glue and marine mussel adhesive protein from *Mytilus edulis* on human osteoblasts and fibroblasts *in vitro*. *Ann. Anat.* **2004**, *186*, 561–566. [CrossRef]

14. Ahmed, T.A.; Giulivi, A.; Griffith, M.; Hincke, M. Fibrin glues in combination with mesenchymal stem cells to develop a tissue-engineered cartilage substitute. *Tissue Eng. Part A* **2011**, *17*, 323–335. [CrossRef] [PubMed]

15. Annabi, N.; Yue, K.; Tamayol, A.; Khademhosseini, A. Elastic sealants for surgical applications. *Eur. J. Pharm. Biopharm.* **2015**, *95*, 27–39. [CrossRef] [PubMed]

16. Sekine, T.; Nakamura, T.; Shimizu, Y.; Ueda, H.; Matsumoto, K.; Takimoto, Y.; Kiyotani, T. A new type of surgical adhesive made from porcine collagen and polyglutamic acid. *J. Biomed. Mater. Res.* **2001**, *54*, 305–310. [CrossRef]

17. Balakrishnan, B.; Soman, D.; Payanam, U.; Laurent, A.; Labarre, D.; Jayakrishnan, A. A novel injectable tissue adhesive based on oxidized dextran and chitosan. *Acta Biomater.* **2017**, *53*, 343–354. [CrossRef] [PubMed]

18. Waite, J.H.; Tanzer, M.L. Polyphenolic substance of *Mytilus edulis*: Novel adhesive containing L-dopa and hydroxyproline. *Science* **1981**, *212*, 1038–1040. [CrossRef] [PubMed]

19. Silverma, H.G.; Roberto, F.F. Understanding marine mussel adhesion. *Biomaterials* **2007**, *28*, 4039–4046.

20. Ninan, L.; Monahan, J.; Stroshine, R.L.; Wilker, J.J.; Shi, R. Adhesive strength of marine mussel extracts on porcine skin. *Biomaterials* **2003**, *24*, 4091–4099. [CrossRef]

21. Ninan, L.; Stroshine, R.L.; Wilker, J.J.; Shi, R. Adhesive strength and curing rate of marine mussel protein extracts on porcine small intestinal submucosa. *Acta Biomater.* **2007**, *3*, 687–694. [CrossRef] [PubMed]

22. Nordqvist, P.; Khabbaz, F.; Malmström, E. Comparing bond strength and water resistance of alkali-modified soy protein isolate and wheat gluten adhesives. *Int. J. Adhes. Adhes.* **2010**, *30*, 72–79. [CrossRef]

23. Liu, Y.; Li, K. Chemical modification of soy protein for wood adhesives. *Macromol. Rapid Commun.* **2015**, *23*, 739–742. [CrossRef]

24. Zhang, L.; An, L.-P.; Zhang, X.T.; Liu, H. Physicochemical properties of soy protein adhesives modified by tartaric acid acylating agent. *Soybean Sci.* **2016**, *95*, 818–823.

25. Hua, Y.; Cui, S.W.; Wang, Q. Gelling property of soy protein–gum mixtures. *Food Hydrocolloids* **2003**, *17*, 889–894. [CrossRef]

26. Chen, H.; Xu, Z.; Mo, J.; Yi, L.; Tang, X.; Shen, X. Effects of guar gum on adhesion properties of soybean protein isolate onto porcine bones. *Int. J. Adhes. Adhes.* **2017**, *75*, 124–131. [CrossRef]

27. Hazirah, M.N.; Isa, M.I.N.; Sarbon, N.M. Effect of xanthan gum on the physical and mechanical properties of gelatin-carboxymethyl cellulose film blends. *Food Packag. Shelf Life* **2016**, *9*, 55–63. [CrossRef]

28. Bemiller, J.N.; Bemiller, J.N. *Carbohydrate Chemistry for Food Scientists*; AACC International: St. Paul, MN, USA, 2007.

29. Carp, D.J.; Bartholomai, G.B.; Relkin, P.; Pilosof, A.M.R. Effects of denaturation on soy protein–xanthan interactions: Comparison of a whipping–rheological and a bubbling method. *Colloids Surf. B Biointerfaces* **2001**, *21*, 163–171. [CrossRef]

30. Lan, D.M.; Zhou, C.X.; Zhang, M.X.; Hong, P.Z. Effect of xanthan gum on emulsion stability on tilapia and soybean protein mixture. *Food Ferment. Ind.* **2016**, *42*, 114–119.

31. Kuo, S.M.; Chang, S.J.; Wang, H.Y.; Tang, S.C.; Yang, S.W. Evaluation of the ability of xanthan gum/gellan gum/hyaluronan hydrogel membranes to prevent the adhesion of postrepaired tendons. *Carbohydr. Polym.* **2014**, *114*, 230–237. [CrossRef] [PubMed]

32. Singh, M.; Tiwary, A.K.; Kaur, G. Investigations on interpolymer complexes of cationic guar gum and xanthan gum for formulation of bioadhesive films. *Res. Pharm. Sci.* **2010**, *5*, 79–87. [PubMed]

33. Taskiajdukovic, K.; Djordjevic, V.; Vidic, M.; Vujakovic, M. Subunit composition of seed storage proteins in high-protein soybean genotypes. *Pesqui. Agropecu. Bras.* **2010**, *45*, 721–729. [CrossRef]

34. Alm, B.; Azevedo, A.; Marques, M.J.; Menossi, M.; Cunha, R.L. Interactions between soy protein isolate and xanthan in heat-induced gels: The effect of salt addition. *Food Hydrocolloids* **2006**, *20*, 1178–1189.

35. Rudolph, N.M.; Agudelo, A.C.; Granada, J.C.; Park, H.E.; Osswald, T.A. WLF model for the pressure dependence of zero shear viscosity of polycarbonate. *Rheol. Acta* **2016**, *55*, 1–9. [CrossRef]

36. Internation, A.S.T.M. *Standard Test Method for Apparent Shear Strength of Single-Lap-Joint Adhesively Bonded Metal Specimens by Tension Loading (Metal-to-Metal)*; Astm International: West Conshohocken, PA, USA, 2010.

37. Chang, Y.Y.; Li, D.; Wang, L.J.; Bi, C.H.; Adhikari, B. Effect of gums on the rheological characteristics and microstructure of acid-induced SPI-gum mixed gels. *Carbohydr. Polym.* **2014**, *108*, 183–191. [CrossRef] [PubMed]

38. Leng, X.J.; Turgeon, S.L. Study of the shear effects on the mixture of whey protein/polysaccharides-2: Application of flow models in the study of the shear effects on wpi/polysaccharide system. *Food Hydrocolloids* **2007**, *21*, 1014–1021. [CrossRef]

39. Zhang, Y.J.; Chen, H.J.; Lü, Y.; Liu, Y.X.; Tang, X.Z.; Shen, X.C. Effects of sodium carboxymethyl cellulose on adhesion properties of soybean protein isolate onto porcine bones. *Sci. Agric. Sin.* **2016**, *49*, 1550–1558.

40. Jiang, Z.; Liu, J.; Jin, L.; Zhang, Q. Extraction and application of Perna viridis foot protein as bioadhesive. *J. Biomed. Eng.* **2010**, *27*, 1266–1273.

41. Wang, J.; Liu, C.; Lu, X.; Yin, M. Co-polypeptides of 3,4-dihydroxyphenylalanine and L-lysine to mimic marine adhesive protein. *Biomaterials* **2007**, *28*, 3456–3468. [CrossRef] [PubMed]

42. Sun, C.; Fantner, G.; Adams, J.; Hansma, P.; Waite, J. The role of calcium and magnesium in the concrete tubes of the sandcastle worm. *J. Exp. Biol.* **2007**, *210*, 1481–1488. [CrossRef] [PubMed]

43. Maurer, P.; Bekes, K.; Gernhardt, C.R. Comparison of the bond strength of selected adhesive dental systems to cortical bone under in vitro conditions. *Int. J. Oral Maxillofac. Surg.* **2004**, *33*, 377–387. [CrossRef] [PubMed]

44. Weber, S.C.; Chapman, M.W. Adhesives in orthopaedic surgery. A review of the literature and in vitro bonding strengths of bone-bonding agents. *Clin. Orthop. Relat. Res.* **1984**, *191*, 249–261.

45. Zhang, J.T.; Yang, X.Q.; Huang, L.X. Changes of viscosity during preparation of soy protein isolate adhesives and their adhesive properties. *China Oils Fats* **2005**, *30*, 68–70.

46. Brewster, V.L.; Ashton, L.; Goodacre, R. Monitoring the glycosylation status of proteins using Raman spectroscopy. *Anal. Chem.* **2011**, *83*, 6074–6081. [CrossRef] [PubMed]

47. Howell, N.; Li-Chan, E. Elucidation of interactions of lysozyme with whey proteins by Raman spectroscopy. *Int. J. Food Sci. Technol.* **1996**, *31*, 439–451. [CrossRef]

48. Dickinson, E.; Euston, S.R. Stability of food emulsions containing both protein and polysaccharide. *Food Polym. Gels Colloids* **1991**, *23*, 132–146.

49. Mc, V.D.L.; Rutten, A.A.; Frens, G. How to develop globular proteins into adhesives. *J. Biotechnol.* **2000**, *79*, 211–221.

50. Abrusán, G.; Marsh, J.A. Alpha helices are more robust to mutations than beta strands. *PLoS Comput. Biol.* **2016**, *12*, e1005242. [CrossRef] [PubMed]

51. Zhang, Z. Urea-modified soy globulin proteins (7S and 11S): Effect of wettability and secondary structure on adhesion. *J. Am. Oil Chem. Soc.* **2007**, *84*, 853–857. [CrossRef]

52. Li-Chan, E.C.Y. The applications of Raman spectroscopy in food science. *Trends. Food Sci. Technol.* **1996**, *7*, 361–370. [CrossRef]

53. Lin, O.H.; Kumar, R.N.; Rozman, H.D.; Mam, N. Grafting of sodium carboxymethylcellulose (CMC) with glycidyl methacrylate and development of UV curable coatings from CMC-g-GMA induced by cationic photoinitiators. *Carbohydr. Polym.* **2005**, *59*, 57–69. [CrossRef]

54. Byler, D.M.; Susi, H. Examination of the secondary structure of proteins by deconvolved FTIR spectra. *Biopolymers* **1986**, *25*, 469–487. [CrossRef] [PubMed]

55. Tcholakova, S.; Denkov, N.D.; Ivanov, I.B.; Campbell, B. Coalescence stability of emulsions containing globular milk proteins. *Adv. Colloid Interface Sci.* **2006**, *123*, 259–293. [CrossRef] [PubMed]

56. Barth, A. Infrared spectroscopy of proteins. *Biochim. Biophys. Acta (BBA) Bioenerget.* **2007**, *1767*, 1073–1101. [CrossRef] [PubMed]

57. Li, C.; Zhu, W.; Xue, H.; Chen, Z.; Chen, Y.; Wang, X. Physical and structural properties of peanut protein isolate-gum arabic films prepared by various glycation time. *Food Hydrocolloids* **2015**, *43*, 322–328. [CrossRef]

58. Toda, H.; Kijima, T. Relation between crystallinity and adhesive property for hemicelluloses from various pulps. *Jpn. Tappi J.* **2010**, *15*, 662–667. [CrossRef]

59. Berg, L.V.D.; Rosenberg, Y.; Van Boekel, M.A.; Rosenberg, M.; Van de Velde, F. Microstructural features of composite whey protein/polysaccharide gels characterized at different length scales. *Food Hydrocolloids* **2009**, *23*, 1288–1298. [CrossRef]

60. Putta, A.; Mottishaw, J.D.; Wang, Z.; Sun, H. Rational design of lamellar π–π stacked organic crystalline materials with short interplanar distance. *Cryst. Growth Des.* **2014**, *14*, 350–356. [CrossRef]

61. Shang, S.; Zhu, L.; Fan, J. Microstructural features of composite whey protein/polysaccharide gels characterized at different length scales. *Carbohydr. Polym.* **2013**, *93*, 561–573. [CrossRef] [PubMed]